Bulletin of the Seismological Society of America, Vol. 95, No. 3, pp. 1027–1044, June 2005, doi: 10.1785/0120040182

Ground Motions for Earthquakes in Southwestern British Columbia and Northwestern Washington: Crustal, In-Slab, and Offshore Events

by Gail M. Atkinson

Abstract Regional ground-motion generation and propagation must be characterized to adequately assess seismic hazard. In the Cascadia region of southwestern British Columbia and northwestern Washington, the ground-motion issues are particularly complex because of the contributions to hazard from five distinct types of events, all of which behave differently in terms of their ground-motion propagation characteristics: (1) shallow earthquakes occurring in the continental crust; (2) shallow earthquakes occurring offshore in oceanic crust; (3) earthquakes occurring within the subducting Juan de Fuca slab beneath the continent (e.g., Puget Sound); (4) earthquakes occurring within the subducting Juan de Fuca slab at the edge of the continent (e.g., transitional events along the west coast of Vancouver Island); and (5) great subduction earthquakes on the interface between the subducting Juan de Fuca plate and the overriding North American plate. In this study, empirical data recorded within the Cascadia region are used to evaluate the source and attenuation characteristics of ground-motion amplitudes from the first four of these event types (crustal, offshore, in-slab, and transitional) and examine their implications for regional ground-motion relations.

For crustal earthquakes in Cascadia, a simple application of the hybrid-empirical approach is used to suggest appropriate regional ground-motion relations. The ground motions are obtained by multiplying California ground-motion relations by a frequency-dependent factor to account for regional differences in crustal amplification. The developed ground-motion relations for Cascadia earthquakes are in reasonable agreement with recorded ground motions in the region. The proposed relations are the first region-specific ground-motion relations to be developed for the Cascadia region, and they provide a useful alternative to California relations for use in seismic hazard analysis.

Introduction

There is growing recognition of the earthquake hazard from both crustal and subduction earthquakes in the Cascadia region of southwestern British Columbia and northwestern Washington. A priority task to enable reliable seismic hazard estimation for the region is the development of region-specific ground-motion relations, which predict average ground-motion amplitudes (response spectra and peak ground acceleration and velocity) as simple functions of earthquake magnitude (moment magnitude, **M**), event type (e.g., crustal or in-slab), and distance. At present, national seismic hazard maps are based on the assumption that ground motions from shallow crustal events in Cascadia may be predicted by using empirical ground-motion relations developed for California, whereas ground motions from large subduction events (interface and in-slab) may be predicted based on empirical relations developed from a global subduction database (Frankel *et al.*, 1996, 1999; Adams and Halchuk, 2003). These assumptions were born more of necessity than knowledge and should be critically evaluated with regional ground-motion data. It is important to understand regional differences in ground-motion generation and propagation and differences between event types within the region to adequately assess seismic hazard. In the Cascadia region, the situation is particularly complex because of the contributions to hazard from five distinct types of events, all of which behave differently in terms of their ground-motion propagation characteristics (Ristau *et al.*, 2003): (1) shallow earthquakes occurring in the continental crust; (2) shallow earthquakes occurring offshore in oceanic crust; (3) earthquakes occurring within the subducting Juan de Fuca slab beneath the continent (e.g., Puget Sound); (4) earthquakes occurring within the subducting Juan de Fuca slab at the continental margin (along the west coast of Vancouver Island); and (4) great subduction earthquakes on the interface between the subducting Juan de Fuca plate and the overriding North American plate.

The purpose of this study is to use empirical data recorded within the Cascadia region to examine the source and attenuation characteristics of ground-motion amplitudes from the first four of these event types (crustal, offshore, transitional, and in-slab). Subduction events on the interface are not addressed in this article because there are no empirical data from Cascadia for this event type; for interface events, we are forced to rely on inferences from the global database (Youngs *et al.*, 1997; Atkinson and Boore, 2003). The approach taken in this study is to use the results of empirical analyses of Cascadia data to formulate the basic assumptions required to develop regional ground-motion relations for the different event types, following the hybrid-empirical approach (Atkinson, 2001; Campbell, 2003). The hybrid-empirical approach is adopted because the analyses of the source and attenuation characteristics in Cascadia suggest that this method is ideally suited to this application. Ground-motion relations are developed by this approach for crustal earthquakes and validated by using response spectra from regional earthquakes of moment magnitude (**M**) ≥4 at distances up to 300 km. Significant uncertainties in regional ground-motion relations remain because of limitations of the database at large (**M** ≥5.5) magnitudes.

Ground-Motion Database

The ground-motion database for the Cascadia region has been growing steadily during the past decade because of increased numbers of broadband seismographic and strong-motion instruments and the occurrence of a few strong earthquakes such as the **M** 6.8 Nisqually, Washington, earthquake in 2000; however, the empirical database is still dominated by small to moderate events (**M** <6), especially in the case of crustal earthquakes. The seismographic database includes older short-period vertical-component data recorded in the 1980s and early 1990s, along with three-component broadband data recorded mostly within the past 5 years. Broadband seismographic data were collected from the Canadian National Seismographic Network (CNSN) and the U.S. National Seismographic Network (USNSN) via their automatic data-request management tools (autodrm); older short-period data were compiled by Atkinson (1995). Strong-motion data have been collected for a few moderate-to-large events, most notably the Nisqually event (data from compilation of Atkinson and Boore, 2003). Figure 1 shows the location of study events, and Figure 2 shows the distribution of seismographic data compiled for this study in magnitude and distance. The distance measure is hypocentral distance, which is appropriate for the small magnitudes that dominate the data. In-slab events were distinguished from crustal or offshore events based on focal depth, combined with geographic location and information on structure from the geophysical profiling of Hyndman *et al.* (1996). Events with depths of greater than 40 km in the Puget Sound area can

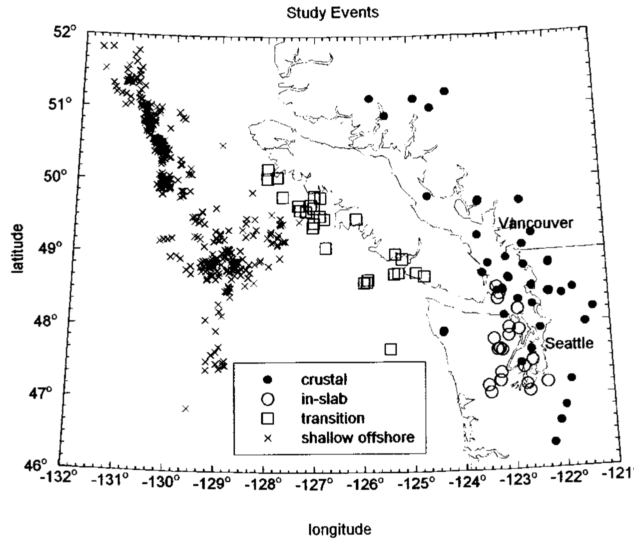

Figure 1. Location of study events, showing crustal (filled circles), in-slab (open circles), transition (squares), and offshore (×) events.

be confidently classified as in-slab. By contrast, because of uncertainties in focal depths and subduction geometry, it is possible that some of the events just west of Vancouver Island at depths of 30 to 40 km may actually be a little above the subducting slab, rather than within it. Furthermore, the in-slab events west of Vancouver Island may exhibit different attenuation characteristics than those beneath Puget Sound because of the different nature of the travel paths. As shown on Figure 2, the events that appear to be within the slab were subdivided into two groups: (1) events beneath the continent, in the Puget Sound region, most of which have depths of 40 to 60 km; and (2) "transition" events, mostly at depths of 25 to 40 km, just west of Vancouver Island. Shallow events are either crustal continental events or offshore (oceanic) events, depending on their location.

Not all the data points plotted on Figure 2 represent broadband three-component data. Of the total database of more than 15,000 records, about 1000 are short-period vertical components. The short-period records make up about 10% of the 5000 records for **M** >4 events, but of the limited dataset for shallow crustal earthquakes, most of the records are short period (800 vertical components, 400 horizontal components). The short-period vertical-component records are thus particularly important for the shallow crustal earthquakes. Almost all the records considered in this study were recorded on hard-rock sites (National Earthquake Hazards Reduction Program [NEHRP] site class A or B), except for a few hundred soil recordings, most of which were from the Nisqually earthquake. Note that the distribution of data with distance is generally good beyond 40 km but poor at closer distances. This places significant constraints on the use the empirical database in ground-motion studies.

The seismographic data were processed as described by Atkinson and Mereu (1992) and Atkinson (2004). In brief, for each record, the window of strongest shaking (shear window, including direct, reflected, and refracted phases) was selected, and a 5% taper was applied at each end of the window. The Fourier spectrum of acceleration was determined, correcting for instrument response. The spectra were smoothed and tabulated over increments of 0.1 log frequency units, for log frequencies of −1 to 1.3 (e.g., 0.1 to 20 Hz) where available. Spectra for a pre-event noise window, normalized to the same duration as the signal window, were processed and tabulated in the same manner. Data were retained for further analysis only at frequencies for which the signal-to-noise ratio exceeds two. Finally, the compiled Fourier spectral data were checked to eliminate data in magnitude-distance ranges affected by low-amplitude "quantization noise" problems (Atkinson, 2004). The main use of the Fourier amplitude spectral database is in the investigation of the source and attenuation characteristics of the events. To focus on these effects, Fourier spectral data were compiled only for hard-rock sites. Data in the range of magnitudes and distances shown in Figure 2 were considered.

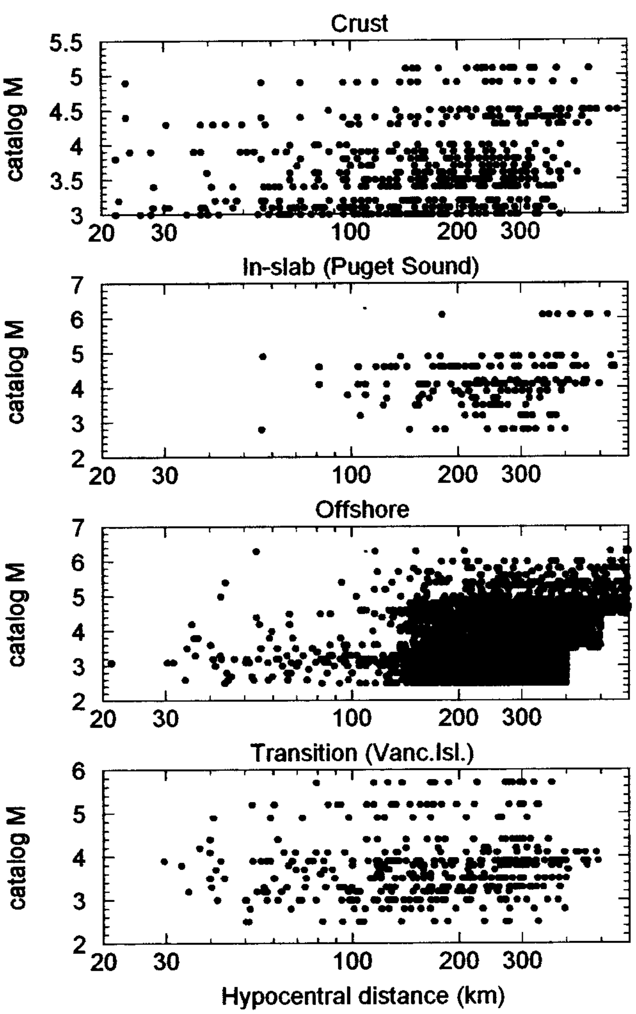

Figure 2. Distribution of Fourier spectra database in magnitude and distance for crustal, in-slab, offshore, and transition events.

To compile a response-spectra database to be used later in validation of ground-motion relations, both rock and soil observations were compiled for events of **M** ≥4 at distances up to 300 km. Response spectra (pseudoacceleration) were computed for 5% damping from the corrected acceleration records. Table 1 lists the events for which response spectra data were compiled. Moment magnitudes are from Ristau (2004) for most events, or from published values for large

Table 1
List of Earthquakes of **M** >4 with PSA Data at R <300 km

Day	Mo	Year	nrec	it	Depth (km)	**M**	m_1
13	4	1949	4	2	54	6.8	
29	4	1965	8	2	60	6.7	
14	2	1981	3	1	7	5.3	5.1
16	6	1986	8	4	35	5.5	5.1
5	3	1989	17	2	46	4.6	4.3
18	6	1989	13	2	45	4.5	4.1
12	9	1989	15	4	34	4.6	4.3
24	12	1989	4	1	18	4.4	4.3
2	4	1990	17	1	1	4.6	4.3
14	4	1990	17	1	2	4.9	4.6
25	4	1992	30	1	11	7.1	
21	9	1993	2	1	6	6.0	
3	1	1994	12	4	28	5.7	4.7
3	5	1996	17	1	4	5.1	
25	6	1998	3	3	10	5.3	4.1
30	8	1998	5	3	10	6.2	5.3
1	9	1998	4	3	10	4.6	4.2
3	7	1999	20	2	41	5.8	4.9
11	12	1999	19	2	53	4.9	3.9
30	4	2000	16	3	10	5.4	4.7
15	5	2000	13	3	10	5.3	4.2
15	5	2000	12	3	10	5.3	4.2
10	6	2000	12	3	10	5.0	4.4
1	8	2000	22	4	41.3	4.9	4.5
11	1	2001	9	3	10	6.0	4.6
23	1	2001	10	3	10	5.5	4.2
23	1	2001	17	3	10	5.7	4.4
17	2	2001	7	3	20	5.0	4.6
17	2	2001	7	3	20	5.3	4.8
17	2	2001	7	3	20	6.3	6.4
28	2	2001	164	2	52	6.8	
7	4	2001	20	4	32.1	4.2	3.9
10	4	2001	9	3	10	5.3	4.6
2	5	2001	6	3	10	5.4	4.3
10	6	2001	15	2	44.6	5.0	4.3
22	7	2001	8	2	50.3	4.1	3.8
20	10	2001	23	4	38.3	4.1	3.7
20	2	2002	14	3	10	5.1	4.2
17	8	2002	32	1	10	4.5	4.3
5	9	2002	10	3	20	5.2	4.9
21	9	2002	42	1	26.2	4.3	3.9
30	10	2002	9	3	20	5.0	4.2
3	11	2002	12	3	10	5.8	5.0
25	4	2003	50	2	51.3	4.6	4.1
1	7	2003	20	3	10	5.0	4.0
19	12	2003	15	3	10	5.4	
17	3	2004	58	1	1.3	4.2	

nrec, number of records; it, 1 for crust, 2 for in-slab (Puget), 3 for offshore, and 4 for transition (Vancouver Island) events (Atkinson and Boore, 2003). I have included the **M** 7.1 1992 Cape Mendocino earthquake as a crustal event. As discussed by Atkinson and Boore (2003), this event might have been either a crustal or subduction interface event; I classify it as crustal purely for expediency here, because there are no other Cascadia interface data to analyze. Both vertical and horizontal components were compiled. There are 835 records of **M** $\geq$4 at $R \leq 300$ km in the response spectral database, 643 of which were recorded on rock.

Attenuation and Source Characteristics of Cascadia Earthquakes

Regression analyses of the Fourier amplitude spectra are used to determine the attenuation characteristics of crustal, in-slab, transition, and offshore events and infer the gross characteristics of their source radiation. Regression is performed by the maximum-likelihood method with the algorithm of Joyner and Boore (1993, 1994). Because of the wealth of vertical-component data and their predominance for the shallow crustal earthquake dataset, the regressions initially focus on the vertical component. The horizontal component is addressed later by examining the residuals obtained when the vertical-component regression equation is used to predict the horizontal-component amplitudes.

Initial inspection of the data indicates that the four data types may exhibit distinct attenuation characteristics and thus need to be regressed separately. This can be seen in Figure 3, which shows a plot of amplitudes versus distance for a subset of the data having catalog magnitude 3.0 to 3.5 (where the catalog magnitude is generally M_L for crustal and in-slab events, and m_b for offshore events). Ristau *et al.* (2003) have noted that offshore events (possibly including the transition events) do not propagate efficiently into the continental crust and therefore have reduced amplitudes and reduced catalog magnitudes, relative to crustal events of the same moment magnitude. Thus, the offshore events plotted on Figure 3 would actually be associated with a larger moment magnitude (as much as 1 unit larger) than the crustal or in-slab events in the figure. Several interesting features can be observed on Figure 3. The crustal events have a distinct attenuation shape with relatively little attenuation in the 80- to 150-km distance range. This feature suggests that a trilinear attenuation form similar to that noted in eastern North America by Atkinson and Mereu (1992) and Atkinson (2004) may be required to adequately model the attenuation over a broad range of distances. The trilinear form represents direct-wave attenuation to about 100 km, followed by a flattening, most likely because of postcritical reflections and refractions from the Moho and other internal discontinuities (Burger *et al.*, 1987). At distances beyond about 200 km, the signal is dominated by the *Lg* phase, consisting of multiply reflected and refracted shear waves (Ristau, 2004). The attenuation behavior varies with distance according to these arrivals. There may also be a transition zone in attenuation behavior for the other event types, although it is not readily

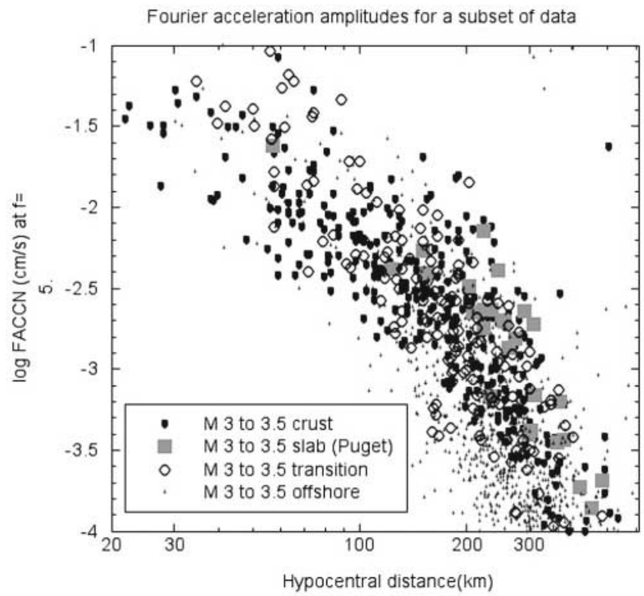

Figure 3. Fourier spectral amplitudes ($f = 2$ Hz) for earthquakes of catalog magnitude 3.0 to 3.5.

apparent on Figure 3. At large distances, beyond about 250 km, the attenuation rate appears to be approximately the same for all types of events. At large distances, the signal consists of multiple reflections and refractions traveling in the crustal wave guide and will attenuate similarly regardless of the origin of the source (Ristau *et al.*, 2003).

For each dataset (vertical components for crustal, in-slab, transition, and offshore events), I fit the observed Fourier amplitudes at each frequency to an equation of the general form:

$$\log A_{ij} = c_1 + c_2 (M_i - 4) + c_3 (M_i - 4)^2 + b \log R_{ij} + c_4 R_{ij} \quad (1)$$

where A_{if} is the observed spectral amplitude of earthquake i at station j, R_{ij} is hypocentral distance, b is the geometric spreading coefficient, and c_1 through c_4 are the other coefficients to be determined. M is a magnitude measure. The most commonly available magnitude for the events from the earthquake catalogs is M_L for the crustal events and m_b for the offshore events. But the catalog contains a mixture of magnitudes, including also M_S for some of the larger events, and M_c (coda magnitude) for some of the crustal events in Washington. The optimal magnitude measure is moment magnitude (**M**) but this is available only for the larger events ($M > 4$) since 1995 (Ristau, 2004), plus a few large older events. I therefore follow the approach taken in Atkinson (2004) and use the intermediate spectral magnitude measure m_1 (Chen and Atkinson, 2002) as the predictive magnitude variable in the regressions to determine the attenuation characteristics. I choose m_1 because it is simple to determine from the data and provides a uniform characterization of overall amplitude level for all events on a common scale. In most regions, m_1 has been shown to be closely related to **M** for moderate events (Chen and Atkinson, 2002; Atkinson, 2004; Motazedian and Atkinson, 2005). The relationship between m_1 and **M** is examined later for events with known moment magnitude.

The magnitude m_1 is defined from the average 1-Hz Fourier acceleration amplitude at a reference distance of 10 km (Chen and Atkinson, 2002). Thus, we need to know the 1-Hz attenuation model to correct observations back to the reference distance of $R = 10$ km To do this in a practical way that ensures stable m_1 estimates, I first do a simple regression to equation (1) for the entire dataset (all types of events) at 1 Hz, with a fixed value of $b = 1$, and by using the catalog magnitude as the magnitude variable; the regression determines that the best value of c_4 for the region is given by $c_4 = -0.0016$. The log 1-Hz amplitude for each record can thus be corrected back to the reference distance of 10 km by using $\log (A_1)_{10} = \log A_1 + \log (R/10) + 0.0016\ R$. An average of the distance-corrected log 1-Hz amplitude values over all stations that recorded the event (denoted $\log(A_1)_{10}$) is used to define m_1 (Chen and Atkinson, 2002):

$$m_1 = 4.4665 + 0.7817 \log (A_1)_{10} + 0.1399 (\log (A_1)_{10})^2 + 0.0351 (\log (A_1)_{10})^3 \quad (2)$$

The next stage of the regression exploits the observation that the attenuation rate is common to all event types at large distances. I assume that attenuation beyond 250 km for all events can be modeled by equation (1) with $b = -0.5$, corresponding to surface-wave spreading in a half-space. The anelastic coefficient, c_4, is inversely related to the quality factor, Q:

$$Q = -(\pi f) / (\ln (10)\ c_4\ \beta) \quad (3)$$

where β is the shear-wave velocity (e.g., Atkinson and Mereu, 1992). I regress the Fourier spectral amplitudes for just the observations beyond 250 km to determine the coefficient c_4 (see values plotted in Fig. 5). By equation (3), the regional quality factor (between approximately 0.5 and 15 Hz) is given by:

$$Q = 229\ f^{0.60} \quad (4)$$

With the distant attenuation (and coefficient c_4) established, I then look in detail at the attenuation for the crustal, in-slab, transition, and offshore datasets separately. I modify equation (1) to allow the coefficient b to take on different values in different distance ranges, to accommodate the geometric attenuation behavior of the shear window as different phases arrive. A hinged trilinear form with hinges at distances r_{t1} and r_{t2} is assumed. Thus, the regression equation can be expressed as:

$$\begin{aligned}
\log A_{ij} &= c_1 + c_2 (M_i - 4) + c_3 (M_i - 4)^2 + b \log R_{ij} + c_4 R_{ij} \qquad R_{ij} \le r_{t1} \\
\log A_{ij} &= c_1 + c_2 (M_i - 4) + c_3 (M_i - 4)^2 + b \log r_{t1} + t \log(R_{ij}/r_{t1}) + c_4 R_{ij} \qquad r_{t1} < R_{ij} \le r_{t2} \\
\log A_{ij} &= c_1 + c_2 (M_i - 4) + c_3 (M_i - 4)^2 + b \log r_{t1} + t \log(r_{t2}/r_{t1}) - 0.5 \log(R_{ij}/r_{t2}) + c_4 R_{ij} \qquad R_{ij} > r_{t2}
\end{aligned} \quad (5)$$

The regression for each dataset determines the values for the coefficients c_1, c_2, c_3, b, t, r_{t1}, and r_{t2} (Table 2). These coefficients describe the best value for the attenuation slope b in the distance range from $R \le r_{t1}$, the best value of the slope at $r_{t1} < \mathrm{R} \le r_{t2}$ (the value of the attenuation slope in the transition zone is denoted t to avoid confusion with b) and the values for the transition distances r_{t1} and r_{t2}. In all cases the attenuation beyond the distance r_{t2} is assumed to be given by a slope of -0.5, with the fixed c_4 values determined in the first step (see Fig. 5). The solution is the set of values that minimizes the average total error, where the error of each observation is measured as the absolute value of the observed log amplitude minus the predicted log amplitude. Note that this scheme covers the possibility of a hinged bilinear model (single transition distance) as well as the hinged trilinear model; for a bilinear model, the solution would indicate that the two transition distances were close together or that the slopes b and t were similar.

Initial regressions indicated that the observed attenuation is complex for each dataset, probably due to the complicated crustal and subcrustal structure in the region. To obtain a satisfactory fit to the data at all frequencies and distances, it is necessary to allow the attenuation coefficients c_1, c_2, c_3, b, and t to be frequency dependent. However, the hinge distances in the attenuation shape, r_{t1} and r_{t2}, are constrained to be the same over all frequencies. Within the crustal dataset, the effect of focal depth on the attenuation residuals was investigated but found to be not significant. Thus, it is not necessary to consider focal depth as an additional predictive variable. The final attenuation model, presented in the next section, provides an excellent distribution of residuals over all distances and all frequencies. This is illustrated for the crustal earthquakes at a frequency of 2 Hz in Figure 4.

Attenuation Results

The attenuation coefficients determined by regression are plotted versus frequency in Figure 5. The values of all coefficients are provided in Table 2. The coefficients can only be determined for frequencies $\ge$0.5 Hz because of the paucity of data at lower frequencies. Note that the attenuation coefficients vary significantly between event types, as do the transition distances. However, within a given distance range the net attenuation is not necessarily distinguishable

Table 2
Coefficients of Regression (Equation 5)

f (Hz)	c_1	c_2	c_3	b	t	c_4
Crust			r_{t1} = 90 km	r_{t2} = 300 km		
0.50	−1.593	1.317	−0.232	−0.466	−0.275	−0.00078
0.63	−1.019	1.479	−0.116	−0.606	−0.294	−0.0009
0.79	−0.252	1.474	−0.157	−0.934	−0.109	−0.0013
1.00	0.424	1.304	−0.024	−1.246	0.143	−0.0018
1.26	0.478	1.274	−0.048	−1.134	−0.039	−0.0022
1.59	0.391	1.283	−0.037	−0.987	−0.028	−0.0026
2.00	0.258	1.202	0.032	−0.862	−0.060	−0.0029
2.51	0.261	1.108	0.000	−0.791	−0.245	−0.0031
3.16	0.320	1.049	0.039	−0.782	−0.458	−0.0032
3.98	0.638	0.923	−0.009	−0.929	−0.504	−0.0034
5.01	0.439	0.864	−0.046	−0.804	−0.787	−0.0034
6.31	0.480	0.850	0.010	−0.818	−1.122	−0.0033
7.94	0.388	0.810	0.074	−0.818	−1.216	−0.0034
10.00	0.594	0.804	0.141	−0.953	−1.300	−0.0035
12.59	0.866	0.821	0.200	−1.156	−1.774	−0.0027
15.85	0.833	0.612	0.108	−1.228	−3.335	−0.0013
19.95	0.712	0.764	0.419	−1.280	−3.731	−0.00044
In-slab (Puget Sound)			r_{t1} = 40 km	r_{t2} = 300 km		
0.50	−2.027	1.670	0.178		−0.867	−0.00078
0.63	−1.842	1.411	0.141		−0.766	−0.0009
0.79	−1.698	1.420	−0.120		−0.668	−0.0013
1.00	−1.493	1.459	−0.236		−0.630	−0.0018
1.26	−1.262	1.384	−0.243		−0.667	−0.0022
1.59	−1.187	1.298	−0.291		−0.516	−0.0026
2.00	−1.042	1.233	−0.327		−0.549	−0.0029
2.51	−0.800	1.198	−0.220		−0.771	−0.0031
3.16	−0.758	1.194	−0.095		−0.811	−0.0032
3.98	−0.765	1.164	−0.208		−0.658	−0.0034
5.01	−0.559	1.084	−0.253		−0.961	−0.0034
6.31	−0.375	1.028	−0.283		−1.317	−0.0033
7.94	−0.426	0.967	−0.329		−1.351	−0.0034
10.00	−0.356	0.994	−0.391		−1.475	−0.0035
12.59	−0.327	0.956	−0.441		−1.854	−0.0027
15.85	−0.020	1.111	−0.442		−3.115	−0.0013
19.95	−0.629	0.759	−0.492		−2.765	−0.00044
Transition (Vancouver Island coast)				r_{t1} = 100 km	r_{t2} = 170 km	
0.50	−0.043	1.532	0.720	−1.144	−1.376	−0.00078
0.63	−0.021	1.556	−0.065	−1.003	−1.158	−0.0009
0.79	−0.382	1.563	−0.253	−0.733	−1.032	−0.0013
1.00	0.298	1.464	−0.100	−0.990	−1.203	−0.0018
1.26	0.524	1.382	−0.115	−1.000	−1.333	−0.0022
1.59	1.329	1.351	−0.166	−1.348	−1.075	−0.0026
2.00	1.593	1.321	−0.208	−1.433	−1.066	−0.0029
2.51	1.745	1.204	−0.288	−1.480	−1.037	−0.0031
3.16	1.433	1.116	−0.324	−1.319	−1.250	−0.0032
3.98	1.665	1.091	−0.302	−1.437	−1.327	−0.0034
5.01	2.263	1.045	−0.283	−1.777	−1.387	−0.0034
6.31	2.853	0.989	−0.238	−2.114	−1.632	−0.0033
7.94	2.897	0.986	−0.113	−2.170	−1.768	−0.0034
10.00	3.214	0.920	−0.174	−2.350	−1.915	−0.0035
12.59	3.046	0.922	−0.078	−2.361	−2.346	−0.0027
15.85	2.709	0.855	0.009	−2.337	−3.202	−0.0013
19.95	3.203	0.979	0.045	−2.681	−3.189	−0.00044
Offshore			r_{t1} = 140 km	r_{t2} = 2 60 km		
0.50	−1.560	1.312	−0.113	−0.173	−2.095	−0.00078
0.63	−1.434	1.400	−0.179	−0.206	−2.173	−0.0009
0.79	−1.089	1.472	−0.206	−0.307	−2.045	−0.0013
1.00	−0.881	1.479	−0.187	−0.338	−1.926	−0.0018

(*continued*)

Table 2

Continued

f (Hz)	c_1	c_2	c_3	b	t	c_4
1.26	−0.452	1.428	−0.165	−0.508	−1.733	−0.0022
1.59	−0.763	1.393	−0.159	−0.300	−1.888	−0.0026
2.00	−0.479	1.344	−0.145	−0.421	−1.787	−0.0029
2.51	−0.427	1.280	−0.140	−0.416	−1.940	−0.0031
3.16	−0.473	1.209	−0.116	−0.401	−2.033	−0.0032
3.98	−0.049	1.161	−0.101	−0.611	−1.963	−0.0034
5.01	0.255	1.096	−0.106	−0.766	−2.214	−0.0034
6.31	0.426	1.048	−0.091	−0.866	−2.460	−0.0033
7.94	0.755	1.033	−0.055	−1.043	−2.510	−0.0034
10.00	0.849	0.972	−0.043	−1.130	−2.409	−0.0035
12.59	1.375	0.908	−0.013	−1.479	−2.929	−0.0027
15.85	1.704	0.866	0.009	−1.757	−3.921	−0.0013
19.95	1.779	0.772	−0.003	−1.934	−4.948	−0.00044

The in-slab attenuation is modeled as bilinear; thus, the value of b is set = 0, with r_{t1} = 40 km; amplitudes at R <40 km are undefined.

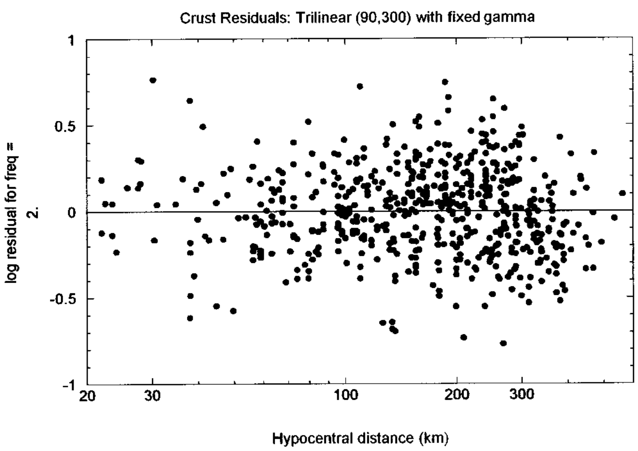

Figure 4. Example of residuals (2 Hz) versus distance for crust dataset (vertical component), for trilinear frequency-dependent regression.

between event types because of the interplay between coefficients. The frequency-dependent trilinear form was adopted after trying various alternatives because it provides trend-free residuals for all the datasets over a broad distance range. (Note: the in-slab model is actually bilinear.)

The obtained model provides a good description of spectral amplitudes over a wide distance range but is not a unique solution. Other combinations of parameters would be obtained for alternative regression model choices. For example, we could allow the attenuation coefficient c_4 to be different for each dataset or select a bilinear or simple linear model rather than a trilinear model. Alternatively, we might constrain the geometric spreading coefficients to be frequency independent. These other possible models might also describe the data well, at least over a given distance and frequency range. The data cannot distinguish which is the "correct" attenuation model because of tradeoffs between different attenuation parameters and between source and attenuation parameters. All that can actually be established is whether a selected model provides a good description of the observed amplitudes, and if so, under what conditions. The model is likely to be reliable if applied within that same validated range of conditions but should not be extrapolated. Thus, we can say that the attenuation model of Table 2 describes vertical-component spectral amplitudes for Cascadia-region events of magnitude 3 to 6, at distances from 40 to 400 km.

To examine the applicability of the attenuation model to the horizontal components, the residuals of the horizontal-component motions, when predicted by the vertical-component equation coefficients of Table 2, are computed (as in Atkinson, 2004). These residuals define the H/V (horizontal-to-vertical) ratio. The H/V ratio calculated from the regression residuals depends on frequency but not on distance. The residuals for each frequency, when regressed against distance, show no significant trend. This indicates that the vertical-component attenuation model also applies to the horizontal component; all this is required is to multiply the vertical-component predictions by the H/V ratio. The H/V ratio is shown versus frequency in Figure 6, and given by:

$$\log \mathrm{H/V} = 0.0566 + 0.0723 \log f \qquad (6)$$

Note that this H/V ratio applies to hard-rock sites only. In general, H/V is believed to be a good, if crude, estimate of site response, as discussed by Lermo and Chavez-Garcia (1993), Beresnev and Atkinson (1997), Atkinson and Cassidy (2000) and Siddiqqi and Atkinson (2002), although not all studies agree on this point (Malagnini *et al.*, 2004). The H/V ratios obtained in this study are consistent with previous results for the region (Siddiqqi and Atkinson, 2002) and conform to the values expected for near-surface shear-wave velocities of about 1.5 km/sec (Atkinson and Cassidy, 2000).

The H/V ratio does not appear to show any trend with

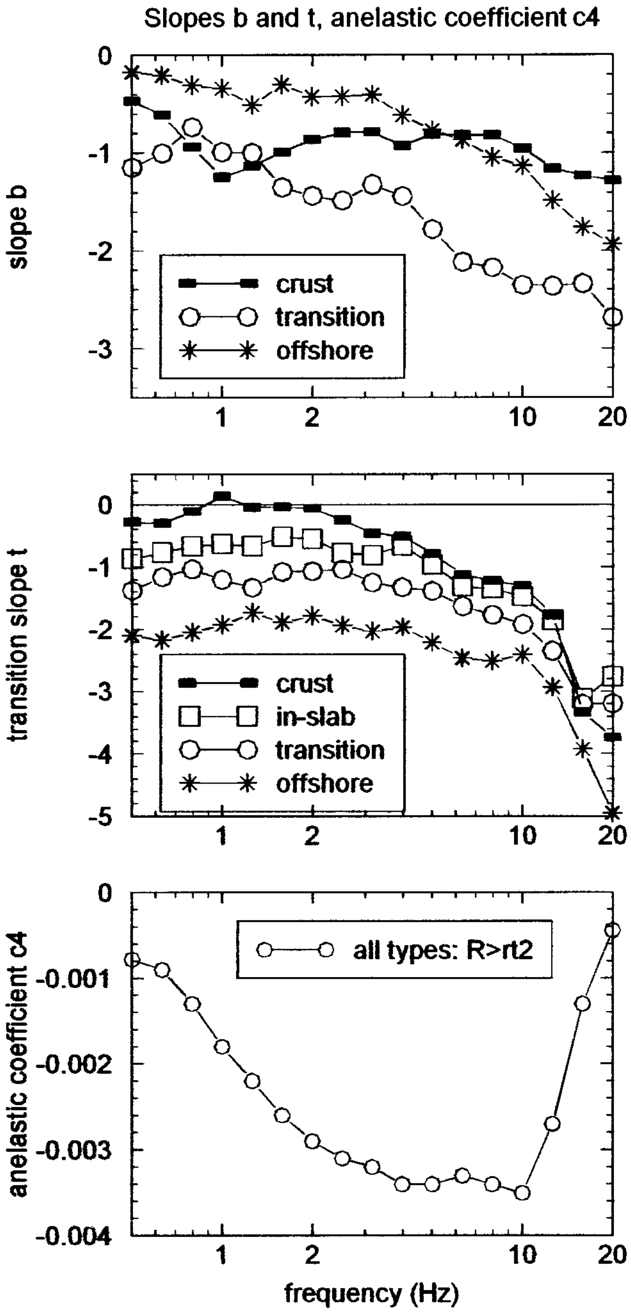

Figure 5. Attenuation coefficients for trilinear regression, showing attenuation slopes b (for $R \leq r_{t1}$) (top) and t (for $r_{t1} < R \leq r_{t2}$) (middle) and anelastic coefficient c_4 (lower).

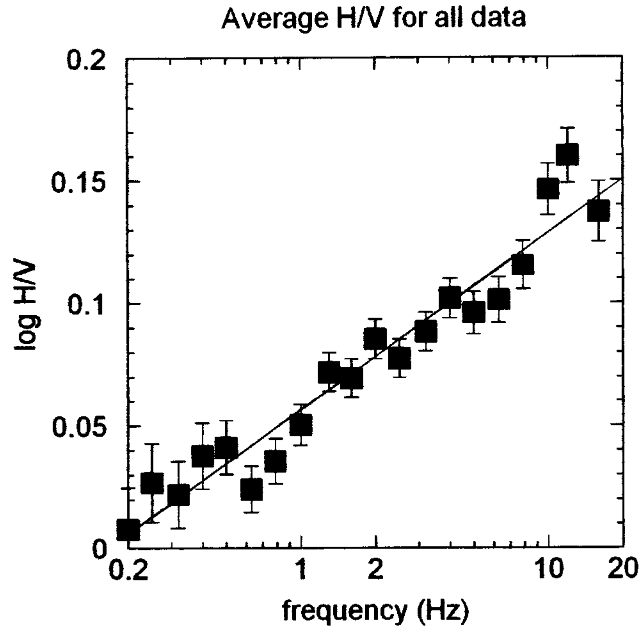

Figure 6. Mean value of log H/V (horizontal-to-vertical component ratio). Symbols show mean and standard error. Line shows best fit by least squares.

distance. This echoes similar observations made in eastern North America (Atkinson, 2004) but is at odds with the expectations of studies based on synthetic waveforms (Herrmann and Malagnini, 2005). On the other hand, the overall attenuation behavior with distance observed in empirical studies does agree with expectations based on synthetics (Herrmann and Malagnini, 2005). The lack of agreement between empirical and synthethic studies in some of these details may reflect complications in the real Earth waveforms that are not completely modeled in the synthetic studies. Alternatively, it may reflect limitations in the empirical database that do not yet allow such trends to be clearly distinguished.

Near-Source Spectral Amplitudes

The database is sparse in the near-source region (Fig. 2). This, combined with the complex frequency-dependent attenuation observed at regional distances, means that we cannot use the regression results to reliably define source characteristics of the radiation. However, we can use the regression results to define the average Fourier spectra at a reference distance of 40 km; this is about as close to the source as we can get given our data distribution. The use of spectra at a reference distance of 40 km follows the approach advocated by Raoof *et al.* (1999), Malagnini *et al.* (2000), and Herrmann and Malagnini (2005) in using regional data to infer source characteristics. The idea is to estimate the spectra at the closest distance that can be obtained reliably, then compare the spectra at that distance with the implications of model predictions.

For each event in the database, we use the attenuation model for that event type (Fig. 5) to project the recorded spectrum back to the reference distance of 40 km:

$$\begin{aligned}
\log A40_{ij} &= \log A_{ij} - b \log R_{ij} - c_4 R_{ij} + F_{40} \qquad R_{ij} \leq r_{t1} \\
\log A40_{ij} &= \log A_{ij} - b \log r_{t1} - t \log (R_{ij}/r_{t1}) \\
&\quad - c_4 R_{ij} + F_{40} \qquad r_{t1} < R_{ij} \leq r_{t2} \qquad (7) \\
\log A40_{ij} &= \log A_{ij} - b \log r_{t1} - t \log (r_{t2}/r_{t1}) \\
&\quad + 0.5 \log (R_{ij}/r_{t2}) - c_4 R_{ij} + F_{40} \qquad R_{ij} > r_{t2}
\end{aligned}$$

where $F_{40} = b \log(40) + c_4(40)$ (note that b and c_4 are negative in sign). The attenuation in the first 40 km that is impled by the b-value is irrelevant in this process, because the effects of that attenuation are removed by the application of the factor F_{40} (i.e., the same attenuation that corrects the amplitudes from 40 km to 1 km is then removed by going from 1 km to 40 km). An average of log spectra is then taken over all N_i stations to obtain the event spectrum at the reference distance of 40 km:

$$\log A40_i = \sum_{j=1}^{N_i} \log A40_{ij}/N_i \qquad (8)$$

Figure 7 compares the reference spectra at 40 km for selected events of **M** 4.5 to 6 with standard 50-bar Brune model spectra at 40 km for **M** 4.5, 5, 5.5, and 6, where the Brune model spectrum is given by (Brune, 1970; Boore, 1983):

$$A_{ij}(f) = C\, M_0(2\pi f)^2/[R(1 + (f/f_0)^2)] \qquad (9)$$

where M_0 is seismic moment, f_0 is corner frequency, and R is distance (40 km). The constant $C = \Re^{\theta\varphi} F\, V/(4\pi\rho\beta^3)$, where $\Re^{\theta\varphi}$ = radiation pattern (average value of 0.55 for shear waves), F = free-surface amplification (2.0), V = partition onto two horizontal components (0.71), ρ = density (2.8 g/cm^3), and β is shear-wave velocity (3.7 km/sec). Corner frequency is given by $f_0 = 4.9e + 6\beta\,(\Delta\sigma/M_0)^{1/3}$, where $\Delta\sigma$ is the stress drop in bars, M_0 is in dyne cm, and β is in kilometers per second (Boore, 1983). In making this comparison, I assume that the vertical-component spectrum is equivalent to the random horizontal-component spectrum before any amplification by the regional velocity gradient or near-surface materials (where the observed H/V ratio represents this amplification). Under this assumption, it is appropriate to compare the vertical-component spectra with an unamplified Brune model for the horizontal component, as per equation (9).

The Brune model is often used in ground-motion modeling as a simple predictive model for source radiation. Note the implicit assumption of simple R^{-1} attenuation from the source to 40 km, corresponding to body-wave spreading in a whole space. It is not known if this attenuation is applicable, although it seems reasonable to assume that the radiation decays in a simple manner close to the source, before regional crustal structure causes the complexities observed in the regional decay rates. From Figure 7, it can be inferred that moderate Cascadia events are consistent with stress drops of less than 50 bars. However, there is much uncertainty in interpreting source parameters from these comparisons because of the complicated attenuation. One way this is manifested is in the apparent mismatch in seismic moment by about 0.5 units at the short-period end of the spectrum (0.5 to 1 Hz). This is likely because of the deteriorating data quality/quantity at frequencies less than 1 Hz, which makes the moment end of the determined spectra unreliable. The lack of smoothness in the obtained spectral shapes at 40 km over all frequencies, and the lack of a clear high-frequency level (5 to 10 Hz) partly reflects the frequency dependence of the attenuation coefficients; the obtained shapes would look slightly different at a different selected reference distance.

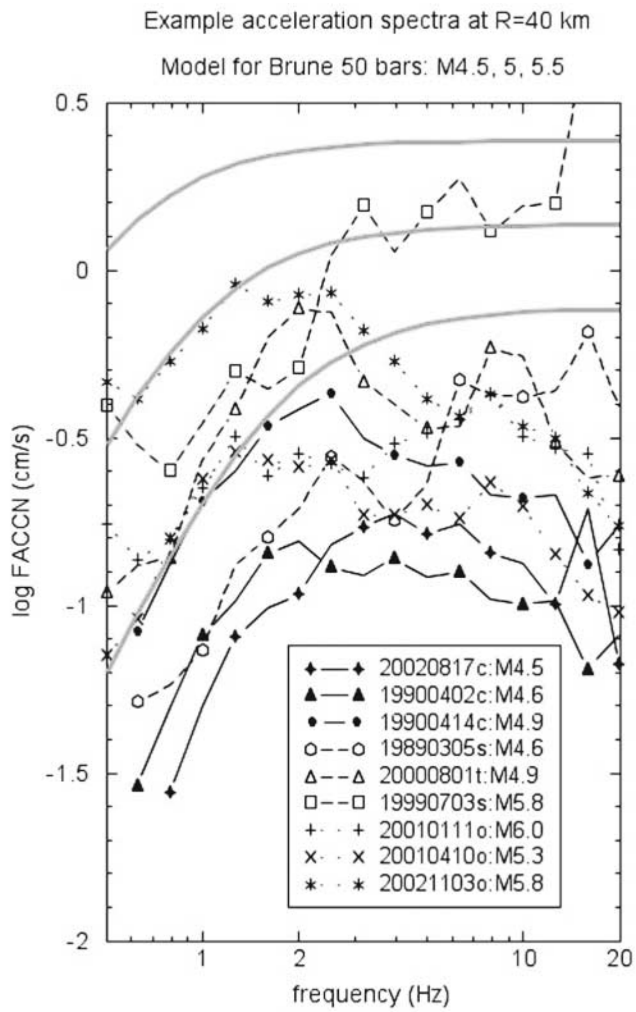

Figure 7. Example of acceleration spectra at reference distance of 40 km for several events of **M** 4.5 to 6 (lines with symbols), in comparison with Brune model spectra with 50-bar stress drop (smooth lines) for **M** 4.5, 5.0, and 5.5. Event legend gives date and moment magnitude of event: c = crustal, s = in-slab, t = transition, o = offshore.

Figure 8 compares the m_1 magnitude values determined in this study with moment magnitudes determined from regional modeling of the long-period waves, as derived by Ristau (2004). The relationship $m_1 = \mathbf{M} - 0.3$ appears reasonable for the crustal events and most of the in-slab events (including the transition events). The offshore events and some of the in-slab and transition events exhibit a different relationship. For the offshore events, $\mathbf{M} - m_1 = 0.7$

on average. This is consistent with findings of previous studies of Ristau *et al.* (2005) and Atkinson and McCartney (2005), which suggest that the relationships between regional and moment magnitudes are different for offshore earthquakes than for continental events.

As a check on the sensitivity of the reference near-source spectra at 40 km to the attenuation model, given the apparent uncertainties noted previously, the regressions were repeated by using just the data within 200 km of the source, along with a simpler functional form. In this simple model, the data for each set were fit to equation (1), assuming a single frequency-independent value of b and allowing the regression to find the best corresponding value of c_4 for each frequency (with separate values of b and c_4 for each event type). This approach provides a reasonable fit to the data at intermediate frequencies and for distances less than 200 km but cannot provide trend-free residuals versus distance at all frequencies. Under this alternative regression model, the attenuation slope b is -1.4 for crustal events, -1.2 for in-slab events, -1.7 for transition events, and -0.1 for offshore events. The associated c_4 values are 0, -0.00037, 0, and -0.0030, respectively, at 1 Hz, decreasing with increasing frequency to -0.0013, -0.0032, -0.0047, and -0.0091 at 10 Hz. The shallow attenuation slope indicated by the b-coefficient for offshore events might appear to suggest very little attenuation for distances less than 200 km, whereas the attenuation of transition events and crustal events is faster than for direct-wave spreading. However, the b-coefficients are somewhat misleading, because the high c_4 values obtained under this model for the offshore events must be considered in assessing the overall attenuation. The net attenuation for the shallow offshore events within the first 200 km is not greatly different than that for the crustal or in-slab events, but the attenuation of the transition events is clearly steeper, suggesting that the deeper events near the continental margin are not propagating efficiently into the continental crust.

Despite a significantly different attenuation model, the inferred spectra at the reference distance of 40 km are consistent with our previous estimates. This is illustrated in Figure 9, which plots the average difference in inferred source terms (at 40 km) versus frequency for the two regression models (simple model minus frequency-dependent trilinear model); the standard deviation of the differences (not shown) is about 0.1 log units for each of the datasets. Note that the dataset is very weak for the in-slab events at R <200 km (Fig. 2). Crustal events have inferred 40-km spectra that agree to within 0.1 log units. Average deviations for other events (in-slab, transition, and offshore) are more variable (up to 0.2 log units), with a tendency for the simple estimates to produce larger inferred spectra at low frequencies, and smaller spectra at high frequencies. The average absolute values of the deviations between models, over all frequencies, is 0.03 log units for crustal events, 0.20 for in-slab, 0.11 for transition, and 0.08 for offshore events. Thus, there is significant uncertainty in near-source amplitudes, but it is certainly less than a factor of two overall. Note that the uncertainty would become larger if the spectra were extrapolated all the way back to the source, beyond the range where the amplitudes are constrained by the data. This is why the definition of near-source spectra at a reference distance of 40 km is a good approach; it results in relatively well-constrained spectra that are not overly sensitive to the adopted form of the attenuation model, as long as the dataset is sufficient.

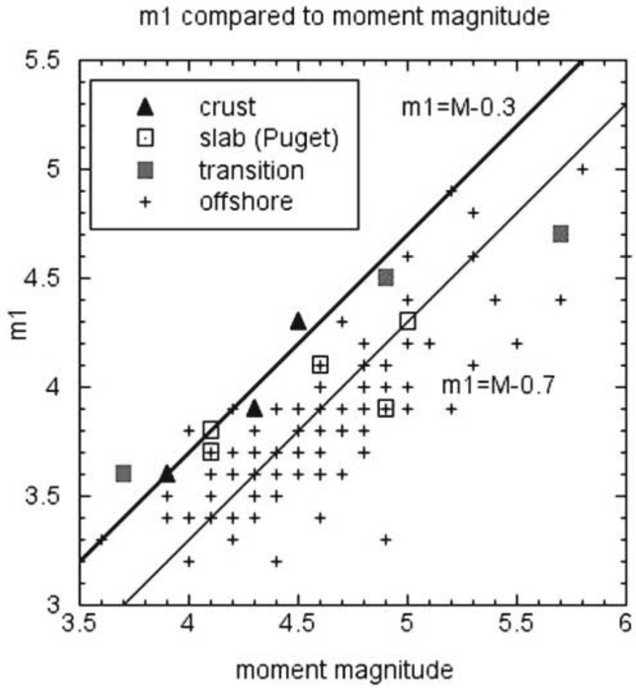

Figure 8. m_1 as determined for events in this study versus moment magnitude, as determined by Ristau (2004). Lines show relationships $\mathbf{M} = m_1 + 0.3$ and $\mathbf{M} = m_1 + 0.7$ for reference.

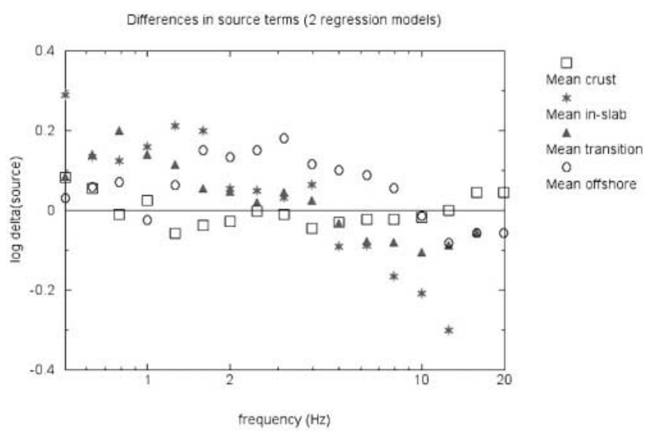

Figure 9. Average difference in source terms at 40-km reference distance for the simple frequency-independent model minus the preferred frequency-dependent trilinear attenuation model.

In summary, event spectra can be obtained from the data at a reference distance of 40 km to within an uncertainty of about 0.1 to 0.2 log units (factor of 1.5), but the use of these spectra to infer source characteristics is subject to significant uncertainty because the attenuation from the source to the reference distance of 40 km is not well understood.

Comparison of Near-Source Spectra for Cascadia versus California

It is useful to know how near-source spectra for earthquakes in Cascadia compare with the better-recorded shallow California earthquakes. Atkinson and Silva (1997) performed regression analysis of the empirical California strong-motion database to obtain a model of the attenuation of Fourier spectral amplitudes. Their results can be used directly to obtain Fourier spectra of California earthquakes at the reference distance of 40 km, for comparison with the events of this study. In making the comparisons, differences between typical site conditions in the two regions must be considered. The Atkinson and Silva (1997) spectra are for motions recorded on soft-rock California sites of NEHRP C category (shear-wave velocity, about 620 m/sec), whereas our spectra are for hard-rock sites of NEHRP A/B category (shear-wave velocity about 1500 m/sec). The fact that the Cascadia region was glaciated in recent history, but California was not, has a significant but predictable influence on average site response for "rock" sites; California rock is not equivalent to Cascadia rock. The amplification factors that apply to typical California soft-rock sites have been evaluated by Boore and Joyner (1997). They provide frequency-dependent factors that represent the amplification of motions through the crustal velocity gradient (from 3.6 km/sec at source depths to 620 m/sec at the surface), combined with near-surface attenuation due to the "kappa" operator (where $\kappa = 0.035$). I adopt their generic soft-rock factors as an estimate of regional site amplification for horizontal-component Fourier spectra recorded on NEHRP C sites in California. Accordingly, I divide the horizontal-component spectra obtained by Atkinson and Silva (1997) for each event, at a reference distance of 40 km, by these factors (listed as FC(CA) in Table 3) to obtain the equivalent unamplified motions. For Cascadia, the reference spectra at 40 km are vertical-component spectra. As mentioned earlier, I assume that vertical-component spectra equal the horizontal-component spectra before amplification through the shear-wave velocity profile; in other words, I assume that the H/V ratio represents regional site amplification for hard-rock sites in Cascadia. This assumption follows the work of Lermo and Chavez-Garcia (1993) and is supported for rock sites by Beresnev and Atkinson (1997) and Atkinson and Cassidy (2000). It is a convenient assumption that appears to work in British Columbia and eastern Canada, although more substantiation of this important assumption would be desirable. Under this assumption, the reference vertical-component spectra for Cascadia can be directly compared with the California reference spectra, divided by California site-amplification factors.

Table 3
Multiplicative Factors to Obtain Cascadia Ground Motions from California Ground-Motion Relations

f (Hz)	FC(CA)	FC(BC)	FC(BC)/FC(CA)
0.1	1.12	1.0	0.892
0.5	1.32	1.08	0.818
0.8	1.46	1.11	0.760
1.0	1.52	1.13	0.743
2.0	1.61	1.17	0.727
3.0	1.57	1.19	0.758
5.0	1.40	1.21	0.864
8.0	1.12	1.21	1.08
10.0	0.96	1.21	1.26
20.0	0.40	1.13	2.82

FC(CA) is the crustal and anelastic attenuation factor for California (soft-rock site), FC(BC) is the corresponding factor for the Cascadia region (hard-rock site in British Columbia), and the resulting factor to apply is FC(BC)/FC(CA).

Figure 10 shows the results of this comparison at four spectral frequencies, based on recordings on rock. In making this plot, I included only those Cascadia events with an independently determined moment magnitude value (Ristau, 2004). Unfortunately, the magnitude-range of overlap between the California and Cascadia data is limited. Nevertheless, the figure supports the hypothesis that Cascadia source parameters for shallow crustal events are approximately equal to (or perhaps slightly less than) California source parameters for shallow crustal events. Perhaps surprisingly, the in-slab and transition-source parameters also appear to follow the same trend, notably including the Nisqually earthquake. This is counter to the typical observation that in-slab events exhibit higher near-source amplitudes than do crustal events (e.g., as suggested by Fig. 14). However, given the large uncertainty (factor of 2) in near-source amplitudes for the in-slab events, the inferred similarity of source parameters for the in-slab events may not be robust. The offshore events have significantly lower source spectral amplitudes than do the California crustal events, with an offset of about 0.5 magnitude units. This offset is fully consistent with the finding that m_l values are about 0.5 to 1 units lower than moment magnitude values. As a generalization, it appears that the near-source amplitudes of offshore events could be predicted by using a California crustal event about 0.5 moment magnitude units lower (e.g., California **M** 6 is equivalent to offshore **M** 6.5).

Ground-Motion Relations for Cascadia

The apparent similarity of near-source amplitudes for crustal earthquakes in Cascadia with those of California earthquakes suggests that trial ground-motion relations can be developed by using a simple hybrid-empirical approach. The hybrid-empirical approach adjusts empirical ground-

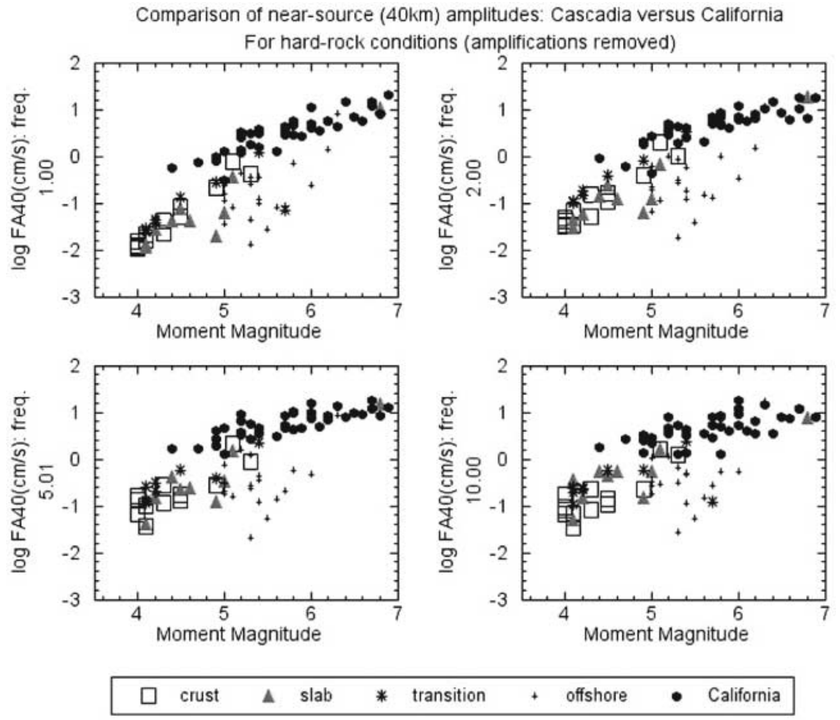

Figure 10. Comparison of Fourier amplitudes at reference distance of 40 km, for hard-rock conditions (all amplifications removed), for California and Cascadia events, for frequencies of 1, 2, 5, and 10 Hz.

motion relations that have been validated for California to be applicable to other regions, by applying factors that account for known regional differences (Campbell, 2003; Atkinson, 2001). All that is required is to account for differences in regional crustal amplification effects (as discussed before) and for any differences in attenuation rates. We can follow the simple approach based on multiplicative factors, as outlined by Atkinson (2001), which works well when there are no differences in source characteristics. (For the offshore events, we can also use the simple approach and adjust for the source differences by using an offset of 0.5 magnitude units [i.e., use **M** 6.5 to predict ground motions for an offshore event of **M** 7].) The use of simple multiplicative factors differs from the Campbell (2003) approach, which uses simulations based on a stochastic model to determine the adjustment factors; the Campbell approach is more general and can more readily handle differences in source spectra, at the cost of additional complexity in application. The simplest hybrid-empirical approach is chosen for Cascadia because it will result in ground-motion relations that have a direct relationship to their California counterparts. The approach mitigates the observed complexities in attenuation that are difficult to fully model with our limited data but can be treated approximately with the hybrid-empirical approach. A more detailed approach to the development of regional ground-motion relations is not warranted because of the inherent limitations of the database, in particular, at larger magnitudes.

To apply the hybrid-empirical method in its simplest form, as proposed by Atkinson (2001), we must develop adjustment factors to apply to California relations to account for: (1) regional crustal amplification and (2) attenuation differences between the two regions. To consider differences in crustal amplification, as discussed earlier we can assume that the amplification for California soft-rock (NEHRP C) sites is given for horizontal components by the generic California rock-amplification factors of Boore and Joyner (1997), with $\kappa = 0.035$. These factors are listed in the FC(CA) column of Table 3. In Cascadia, we assume that the regional amplification for the horizontal component on hard-rock sites (NEHRP A/B) is given by the regional H/V ratio, with $\kappa = 0.011$ (Atkinson, 1995). These factors are listed in the FC(BC) column of Table 3. The relative amplification factor, to apply to horizontal-component California rock relations to predict the corresponding horizontal-component motions on hard rock in Cascadia, is FC(BC)/FC(CA), as given in Table 3. Note that the reference rock condition is different for the two regions. For soil sites in Cascadia, we can apply the generic soil factors from an empirical California ground-motion relation to predict soil motions from the hard-rock motions. For this purpose, I adopt the soil-response terms in the Abrahamson and Silva (1997) ground-motion relations.

The effects of regional differences in attenuation are examined in Figure 11. Figure 11 plots the relative attenuation of Fourier amplitudes in California (from Atkinson and Silva, 1997) in comparison with the attenuation for events in Cascadia, beyond the reference distance of 40 km, by using the frequency-dependent attenuation model developed in this study. Overall differences in attenuation of earthquakes between California and Cascadia are small enough to be neglected within the first 200 km, with the exception

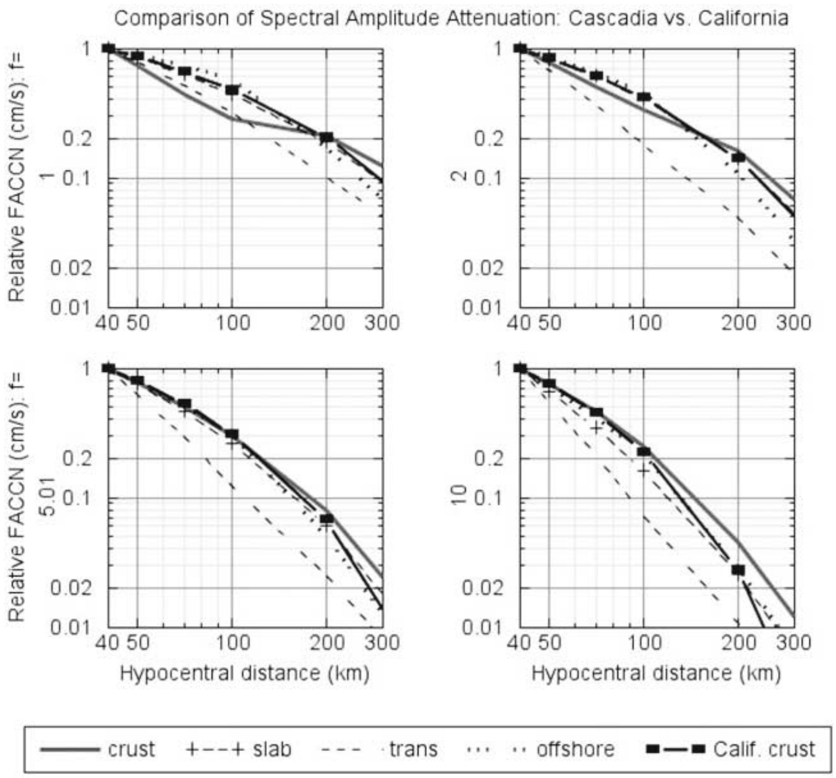

Figure 11. Relative attenuation of Fourier amplitudes for California crustal events (line with symbols) compared to Cascadia events (lines), for frequencies 1, 2, 5, and 10 Hz.

of the transition earthquakes, which attenuate steeply. The first 200 km is the distance range of interest for the development of ground-motion relations for seismic hazard applications. The offshore attenuation is sufficiently similar to the crustal attenuation within 200 km to neglect the differences. Perhaps surprisingly, the in-slab attenuation also appears similar to the crustal attenuation in this distance range. Note that the in-slab data are poor at $R < 200$ km, so this apparent attenuation rate for the in-slab events may not be robust.

I apply the factors outlined previously and given in Table 3 to selected California ground-motion relations to obtain the predicted relations for Cascadia, as follows:

1. For crustal earthquakes, multiply California relations by factor FC(BC)/FC(CA).
2. For offshore earthquakes, multiply California relations for 0.5 **M** unit greater than target magnitude by the factor FC(BC)/FC(CA). (Note: In practice, this offset is counterbalanced by the common convention that assumes $\mathbf{M} = M_L$ for such events, when the actual relation is closer to $\mathbf{M} = M_L + 0.7$ (Ristau *et al.*, 2003; Atkinson and McCartney, 2004). Thus, the common miscalculation of magnitude for offshore events results in predicting lower ground motions, which is equivalent to the approach taken here).

The apparent similarity of Cascadia in-slab source and attenuation parameters to those for the crustal events suggests that the crustal relations might also apply to in-slab events. This hypothesis could be considered as an alternative ground-motion relation in a hazard analysis for the purpose of evaluating uncertainty. However, global relationships for in-slab events based on a larger database (Atkinson and Boore, 2003) should be considered more reliable for such events and accorded greater weight.

The selected California "host relations" for the hybrid-empirical approach are the empirical relations of Abrahamson and Silva (1997) and the empirical-stochastic relations of Atkinson and Silva (2000). The Atkinson and Silva (2000) relations make a useful comparison because they are referenced to a simple seismological model of source and attenuation and are applicable to somewhat lower magnitudes and larger distances than are strictly empirical relations.

The developed horizontal-component ground-motion relations for Cascadia crustal events can be compared with response spectra data (PSA, 5% damped pseudoacceleration), as listed in Table 1. Both horizontal- and vertical-component data may be used in these comparisons, provided vertical-component data are multiplied by the H/V ratio (equation 6). Figure 12 shows an example comparison for crustal events of **M** 4.5 to 5.5 on rock sites. The relations overestimate PSA overall, but the shape of the attenuation is appropriate. The modified Abrahamson and Silva (1997) and the modified Atkinson and Silva (2000) relations are very similar to each other within 100 km of the source. This is true at larger magnitudes also (Atkinson and Silva, 2000). However, the Atkinson and Silva (2000) relations have a slightly better attenuation shape with distance, in terms of

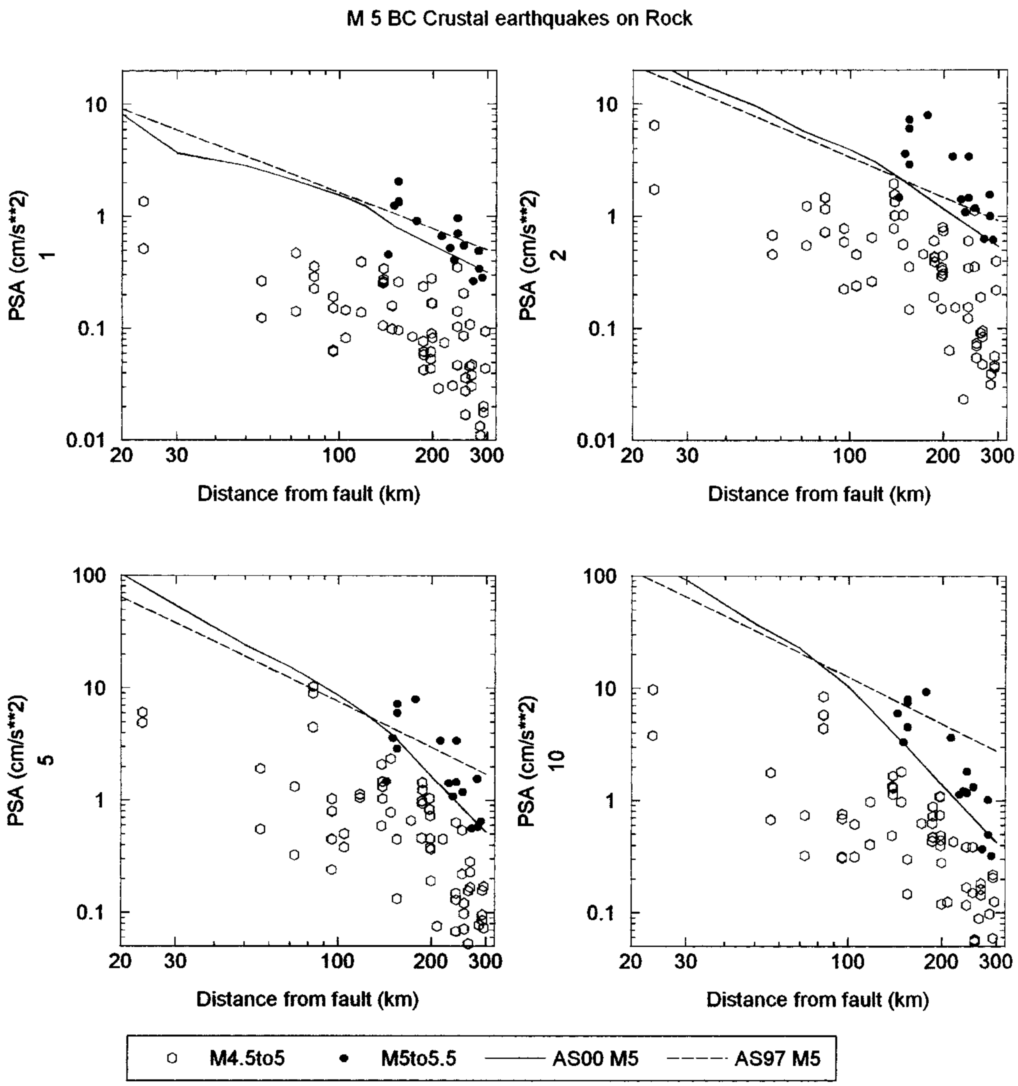

Figure 12. Observed PSA for Cascadia events of **M** 4.5 to 5.5 compared with proposed ground-motion relations for **M** 5, for 1, 2, 5, and 10 Hz. Symbols distinguish events at high and low end of magnitude range.

matching the attenuation shape exhibited by the data. Therefore, in the comparisons that follow I will focus on the modified Atkinson and Silva (2000) relations. For ease of use, the modified relations (after multiplication by the Cascadia factors) have been refit to a standard equation of the form:

$$\text{Log } Y = a_1 + a_2 (\mathbf{M} - 6) + a_3 (\mathbf{M} - 6)^2 + a_4 \log R + a_5 R \quad (10)$$

where $R = \sqrt{(D^2 + h^2)}$, D is the closest distance to the fault (or hypocentral distance for small events) and h is given by $\log h = -0.05 + 0.15\,\mathbf{M}$. Table 4 gives the coefficients of the relations. Note that for offshore events, the coefficients are the same as for crustal events, but the terms ($\mathbf{M} - 6$) in equation (10) are replaced by ($\mathbf{M} - 6.5$) to produce the required 0.5 magnitude unit offset for such events.

The fit of the relations to data is more critical for the larger magnitudes of more relevance to hazard estimation. The fit is examined in various magnitude ranges in Figure 13, which plot the residuals (log observed PSA − log predicted PSA) versus distance by magnitude range. Both vertical-component data (*H/V) and horizontal-component data are included. Soil data are included by using the empirical soil response factors of Abrahamson and Silva (1997) to predict soil motions. I conclude that the developed ground-motion relations of Table 4 provide a reasonable fit to the Cascadia crustal data, although there is clearly overestimation of the response spectra from smaller events (**M** <5). However, it is acknowledged that the database is weak for the magnitude-distance range of interest, and therefore these relations have greater uncertainty than do those in data-rich regions such as California. Nevertheless, a region-specific relation for Cascadia crustal earthquakes, despite its limitations in terms of data validation, is a valuable tool for

Table 4
Regression Coefficients for Cascadia Ground-Motion Relations (Equation 10) on Hard Rock: Crust (and Offshore with Adjustment to **M** in Equation 10)

f (Hz)	a_1	a_2	a_3	a_4	a_5
0.1	1.4172	0.9466	−0.0587	−1.0116	
0.2	2.0247	0.8884	−0.0809	−1.0109	
0.32	2.2116	0.8628	−0.0886	−1.0179	
0.5	2.5913	0.7957	−0.1069	−1.0341	
1	3.1283	0.6818	−0.1158	−1.0925	−0.0002
2	3.5520	0.5615	−0.1031	−1.0977	−0.0013
3.2	3.8160	0.4907	−0.0844	−1.1309	−0.0020
5	4.0439	0.4356	−0.0626	−1.1721	−0.0028
10	4.3732	0.3972	−0.0413	−1.2977	−0.0035
20	4.6827	0.4064	−0.0378	−1.4813	−0.0018
pga	3.9427	0.4182	−0.0446	−1.4070	−0.0014
pgv	2.3557	0.5796	−0.0338	−1.2450	

Recommended value for total standard error (sigma) is that given by Abrahamson and Silva (1997), as shown on Figure 14. For soil sites, the soil-response coefficients as given by Abrahamson and Silva (1997) may be used.

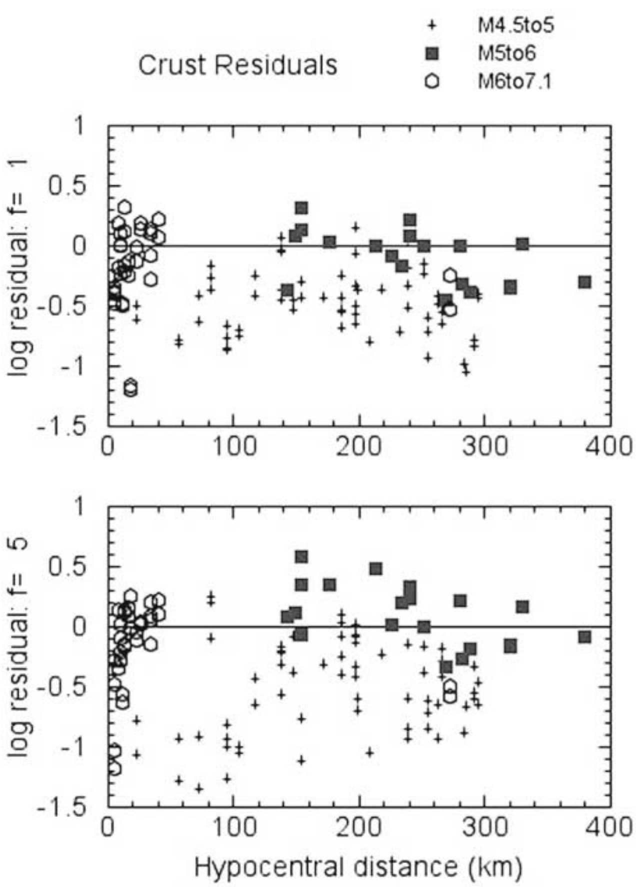

Figure 13. PSA residuals for proposed ground-motion relations for crustal events at 1 and 5 Hz. Symbols distinguish magnitude ranges of data.

regional hazard analysis. Furthermore, the inherent inability to fully validate this relationship against Cascadia crustal data is also a limitation of applying any such relationships (e.g., standard California relations) to Cascadia.

An interesting consequence of the apparent similarity of in-slab source and attenuation characteristics to those for the crustal events is that the developed relationship for crustal earthquakes might also be applicable to in-slab events. However, because of the limitations of the in-slab database for this study, this alternative is not considered very reliable. It is suggested as a possibility for the purposes of evaluating uncertainty in hazard estimates caused by uncertainties in ground motions. Global relationships for in-slab events (Atkinson and Boore, 2003) should be accorded a higher weight.

Figure 14 compares the developed relations for crustal Cascadia earthquakes with empirical relations for California (Abrahamson and Silva, 1997) and with the in-slab relations developed from a global subduction database by Atkinson and Boore (2003), all for rock sites. Cascadia ground motions for crustal events are slightly less than those for California crustal events at low frequencies because of the effects of glaciation on typical rock-site conditions. The Atkinson and Boore (2003) relations predict larger amplitudes for in-slab events at near distances, especially for **M** 7, in comparison with the relations developed in this study (whereas the relations are intended mainly for crustal earthquakes, they might also apply to in-slab events, as discussed earlier). The Atkinson and Boore (2003) relations are considered more reliable for the Cascadia in-slab events because of the larger global database at short distances. The discrepancies observed between the relations serve as a measure of epistemic uncertainty in amplitudes (about a factor of 2).

Uncertainty in Ground-Motion Relations

An important issue for the use of ground-motion relations in seismic hazard analysis concerns their uncertainty. Two types of uncertainty are important: epistemic uncertainty, representing our uncertainty in the correctness of the median, and aleatory uncertainty, representing random variability of observations about the median (Toro and McGuire, 1987). An estimate of the epistemic uncertainty can be obtained by examining Figures 13, 14, and 15. Given the differences between these relations and those for other regions, the discrepancies between the developed relations and data, and our uncertainty in the statement that the source parameters are equivalent across regions, the median relations for events of **M** >5 could be adjusted by as much as plus or minus a factor of 2 and still be consistent with regional data and other considerations. The regional attenuation with distance is reasonably well constrained beyond 40 km, but the possibility exists that attenuation of crustal events within 40 km could differ significantly from that in California. This requires further study with new data and is difficult to quantify at this time.

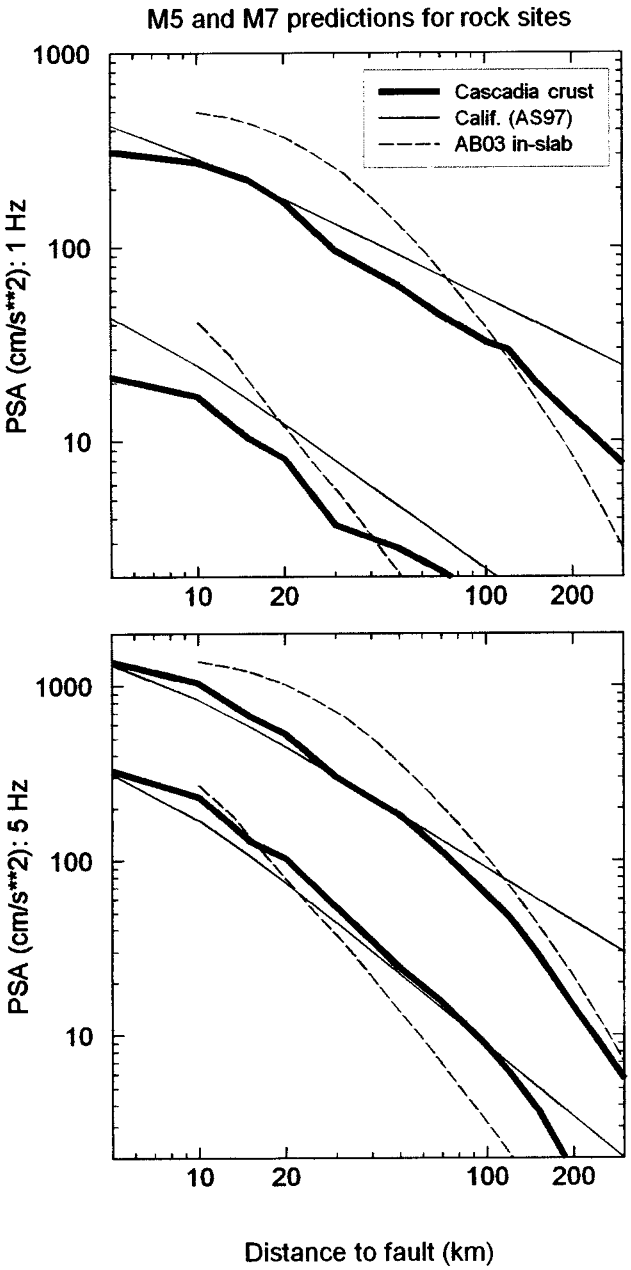

Figure 14. Comparison of Cascadia ground-motion relations (heavy lines) with those of Abrahamson and Silva (1997) for California (light solid line) and Atkinson and Boore (2003) for in-slab events (global database, light dashed line), for 1- and 5-Hz PSA, for events of **M** 5 and 7 on rock.

The aleatory uncertainty can be represented by the standard deviation of the residuals (sigma). This is the total aleatory uncertainty, representing both interevent and intra-event components. Figure 15 plots this variability versus magnitude for Cascadia crustal events in comparison with typical values for California, as given by Abrahamson and Silva (1997) (upper part of the figure). The mean residuals averaged in magnitude ranges are also plotted (lower part of the figure). The large negative mean residuals in Figure 15 are potentially misleading in some cases, because the residuals tend to grow increasingly negative at large distances. Looking at just the limited crustal data for events of **M** $\geq$5 at $R \leq 100$ km, the mean residual is -0.18 at 1 Hz and -0.15 at 5 Hz. Thus, for these cases (**M** $\geq$5 at $R \leq 100$ km), mean residuals indicate an error of less than a factor of 2 overall.

Based on the lack of data for Cascadia at close distances and large magnitudes, and the fact that the overall trend in standard deviations appears to follow that suggested for California, I suggest that aleatory uncertainty should be assumed to equal that for California (e.g., as given in Abrahamson and Silva, 1997). It is a reasonable assumption that variability in amplitudes should be similar in the two regions, because they are driven by the same gross factors (random variability in earth properties, directivity, etc.). On the other hand, it is also possible that variability of ground motion is greater in Cascadia because of the complicated crustal and subcrustal geometry of the subduction zone through which the waves travel.

In summary, in applying the hybrid-empirical ground-motion relations of Table 3, I suggest an overall epistemic uncertainty of a factor of 2, with aleatory uncertainty given by the California sigma values of Abrahamson and Silva (1997).

Conclusions

A simple application of the hybrid-empirical approach may be used to develop regional ground-motion relations for earthquakes in the Cascadia region of southwestern British Columbia and northwestern Washington. Ground-motion relations are suggested for crustal and offshore events. For crustal earthquakes in Cascadia, ground motions are obtained by multiplying California ground-motion relations by a frequency-dependent factor to account for regional differences in crustal amplification. The ground motion from offshore events can be predicted by using the Cascadia crustal relations, but for a one-half moment magnitude unit less (e.g., predict **M** 7 motions by using relations for **M** 6.5). The developed ground-motion relations for Cascadia earthquakes are in reasonable agreement with recorded ground motions in the region. However, ground-motion relations in Cascadia remain highly uncertain because of the complex environment and the lack of regional data in the magnitude-distance range of most engineering interest.

Acknowledgments

This study was supported by National Earthquake Hazards Reduction Program Grant 03HQGR0081. The assistance of graduate students in data processing is gratefully acknowledged, particularly Raymond Casey, Stella Heenan, San Linn Kaka, Aaron Snider, and Eleanor Sonley. I thank Luca Malagnini and an anonymous review for numerous constructive comments that greatly improved the manuscript, and, in particular, for the suggestion made by the anonymous reviewer that in-slab events along the west coast

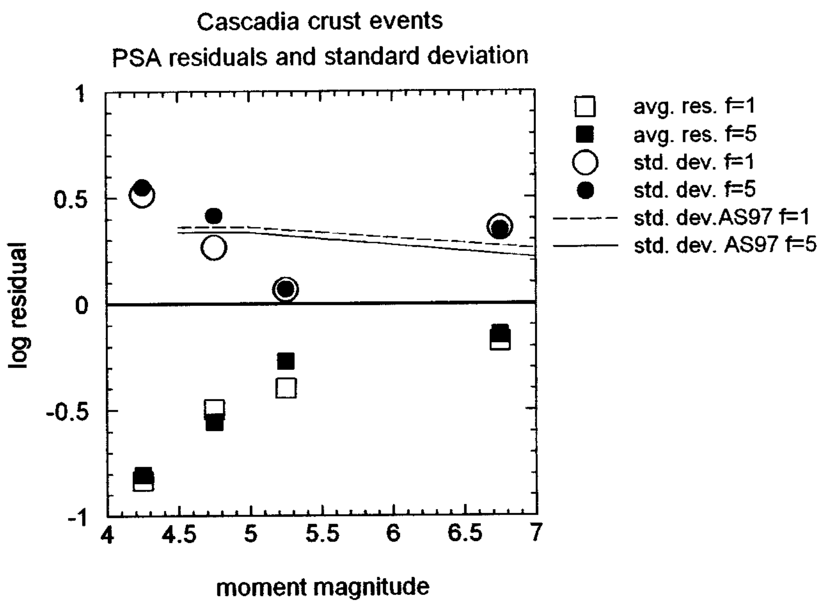

Figure 15. Mean PSA residuals (plot below 0 line) and their standard deviations (plot above 0 line) for crust events at 1 and 5 Hz. Lines show California standard deviations of Abrahamson and Silva (1997).

of Vancouver Island might behave differently in terms of ground-motion characteristics than do in-slab earthquakes beneath Puget Sound.

References

Abrahamson, N., and W. Silva (1997). Empirical response spectral attenuation relations for shallow crustal earthquakes, *Seism. Res. Lett.* **68,** 94–127.

Adams, J., and S. Halchuk (2003). Fourth generation seismic hazard maps of Canada: values for over 650 Canadian localities intended for the 2005 National Building Code of Canada, Geological Survey of Canada Open-File Rept. 4459, 150 pp.

Atkinson, G. (1995). Attenuation and source parameters of earthquakes in the Cascadia region, *Bull. Seism. Soc. Am.* **85,** 1327–1342.

Atkinson, G. (2001). An alternative to stochastic ground motion relations for use in seismic hazard analysis in eastern North America, *Seism. Res. Lett.* **72,** 299–306.

Atkinson, G. (2004). Empirical attenuation of ground motion spectral amplitudes in southeastern Canada and the northeastern United States, *Bull. Seism. Soc. Am.* **94,** 1079–1095.

Atkinson, G., and D. Boore (1997). Stochastic point-source modeling of ground motions in the Cascadia region, *Seism. Res. Lett.* **68,** 74–85.

Atkinson, G., and D. Boore (2003). Empirical ground-motion relations for subduction zone earthquakes and their application to Cascadia and other regions, *Bull. Seism. Soc. Am.* **93,** 1703–1729.

Atkinson, G., and R. Casey (2003). A comparison of ground motions from the 2001 M6.8 in-slab earthquakes in Cascadia and Japan, *Bull. Seism. Soc. Am.* **93,** 1823–1831.

Atkinson, G., and J. Cassidy (2000). Integrated use of seismograph and strong motion data to determine soil amplification in the Fraser Delta: results from the Duvall and Georgia Strait earthquakes, *Bull. Seism. Soc. Am.* **90,** 1028–1040.

Atkinson, G., and S. McCartney (2005). A revised magnitude-recurrence relation for shallow crustal earthquakes in southwestern British Columbia, considering the relationship between moment magnitude and regional magnitude scales, *Bull. Seism. Soc. Am.* **95,** 334–340.

Atkinson, G., and R. Mereu (1992). The shape of ground motion attenuation curves in southeastern Canada, *Bull. Seism. Soc. Am.* **82,** 2014–2031.

Atkinson, G., and W. Silva (2000). Stochastic modeling of California ground motions, *Bull. Seism. Soc. Am.* **90,** 255–274.

Atkinson, G., and W. Silva (1997). Empirical source spectra for California earthquakes, *Bull. Seism. Soc. Am.* **87,** 97–113.

Beresnev, I., and G. Atkinson (1997). Shear wave velocity survey of seismographic sites in eastern Canada: calibration of empirical regression method of estimating site response, *Seism. Res. Lett.* **68,** 981–987.

Boore, D. (1983). Stochastic simulation of high-frequency ground motions based on seismological models of the radiated spectra, *Bull. Seism. Soc. Am.* **73,** 1865–1894.

Boore, D., and W. Joyner (1997). Site amplifications for generic rock sites, *Bull. Seism. Soc. Am.* **87,** 327–341.

Brune, J. (1970). Tectonic stress and the spectra of seismic shear waves from earthquakes, *J. Geophys. Res.* **75,** 4997–5009.

Burger, R., P. Somerville, J. Barker, R. Herrmann, and D. Helmberger (1987). The effect of crustal structure on strong ground motion attenuation relations in eastern North America, *Bull. Seism. Soc. Am.* **77,** 420–439.

Campbell, K. (2003). Prediction of strong-ground motion using the hybrid-empirical method and its use in the development of ground-motion (attenuation) relations in eastern North America, *Bull. Seism. Soc. Am.* **93,** 1012–1033.

Chen, S., and G. Atkinson (2002). Global comparisons of earthquake source spectra, *Bull. Seism. Soc. Am.* **92,** 885–895.

Frankel, A., C. Mueller, T. Barnhard, D. Perkins, E. Leyendecker, N. Dickman, S. Hopper, and M. Hopper (1996). National seismic hazard maps, June 1996. *U.S. Geol. Surv. Open-file Rept. 96-532*.

Frankel, A., C. Mueller, T. Barnhard, D. Perkins, E. Leyendecker, N. Dickman, S. Hanson, and M. Hopper (1999). National seismic hazard mapping project, http://geohazards.cr.usgs.gov.

Herrmann, R., and L. Malagnini (2005). Interpretation of high frequency ground motion from regional seismic network observations, *Bull. Seism. Soc. Am.* (in press).

Hyndman, R., G. Rogers, D. Dragert, K. Wang, J. Clague, J. Adams, and P. Bobrowsky (1996). Giant earthquakes beneath Canada's west coast, *Geosci. Canada* **23,** no. 2, 63–72.

Joyner, W., and D. Boore (1993). Methods for regression analysis of strong-motion data, *Bull. Seism. Soc. Am.* **83,** 469–487.

Joyner, W. B., and D. M. Boore (1994). Erratum to Joyner and Boore (1993), *Bull. Seism. Soc. Am.* **84,** 955–956.

Lermo, J., and F. Chavez-Garcia (1993). Site effect evaluation using spectral ratios with only one station, *Bull. Seism. Soc. Am.* **83,** 1574–1594.

Malagnini, L., R. Herrmann, and M. Di Bona (2000). Ground-motion scaling in the Appenines (Italy), *Bull. Seism. Soc. Am.* **90,** 1062–1081.

Malagnini, L., K. Mayeda, A. Akinci, and P. Bragato (2004). Estimating absolute site effects, *Bull. Seism. Soc. Am.* **94,** 1343–1352.

Motazedian, D., and G. Atkinson (2005). Earthquake magnitude measurements for Puerto Rico, *Bull. Seism. Soc. Am.* **95,** 725–730.

Raoof, M., R. Herrmann, and L. Malagnini (1999). Attenuation and excitation of three-component ground motion in sourthern California, *Bull. Seism. Soc. Am.* **89,** 888–902.

Ristau, J. (2004). Seismotectonics of western Canada from regional moment tensor analysis, *Ph.D. Dissertation*, School of Earth and Ocean Sciences, University of Victoria, Victoria, British Columbia.

Ristau, J., G. Rodgers, and J. Cassidy (2003). Moment magnitude–Local magnitude calibration for earthquakes off Canada's west coast, *Bull. Seism. Soc. Am.* **93,** 2296–2300.

Siddiqqi, J., and G. Atkinson (2002). Ground motion amplification at rock sites across Canada, as determined from the horizontal-to-vertical component ratio, *Bull. Seism. Soc. Am.* **92,** 877–884.

Toro, G., and R. McGuire (1987). Calculational procedures for seismic hazard analysis and its uncertainty in the eastern United States, in *Proc. Third Intl. Conf. Soil Dynamics and Earthquake Eng.*, Princeton, New Jersey, pp. 195–206.

Youngs, R., S. Chiou, W. Silva, and J. Humphrey (1997). Strong ground motion attenuation relationships for subduction zone earthquakes, *Seism. Res. Lett.* **68,** 58–73.

Department of Earth Sciences
Carleton University
Ottawa, Ontario K1S 5B6, Canada

Manuscript received 1 September 2004.